Journal of Energy Chemistry 37 (2019) 163–171

Contents lists available at ScienceDirect

Journal of Energy Chemistry

journal homepage: www.elsevier.com/locate/jechem

http://www.journals.elsevier.com/journal-of-energy-chemistry/

Isomerization of linear C_5–C_7 over Pt loaded on protonated fibrous silica@Y zeolite (Pt/HSi@Y)

S. Triwahyono[a], A. A. Jalil[b,c,*], S. M. Izan[a], N. S. Jamari[a], N. A. A. Fatah[b]

[a] Faculty of Science, Universiti Teknologi Malaysia, 81310 UTM Johor Bahru, Johor, Malaysia
[b] School of Chemical and Energy Engineering, Faculty of Engineering, Universiti Teknologi Malaysia, 81310 UTM Johor Bahru, Johor, Malaysia
[c] Centre of Hydrogen Energy, Institute of Future Energy, Universiti Teknologi Malaysia, 81310 UTM Johor Bahru, Johor, Malaysia

ARTICLE INFO

Article history:
Received 23 October 2018
Revised 23 February 2019
Accepted 28 February 2019
Available online 20 March 2019

Keywords:
Pt/HSi@Y
Fibrous silica
Y zeolite
Acidic sites
C_5–C_7 isomerization

ABSTRACT

A novel fibrous silica Y zeolite (HSi@Y) loaded with Pt has been studied based on its ability to produce protonic acid sites originating from molecular hydrogen. The Pt/HSi@Y was prepared using seed assisted crystallization followed by protonation and Pt-loading. The product formed had a spherical morphology with bicontinuous lamellar with a diameter in the range of 500–700 nm. The catalytic activity of the Pt/HSi@Y has been assessed based on light linear alkane (C_5–C_7) isomerization in a micro-catalytic pulse reactor at 423–623 K. A pyridine IR study confirmed that the introduction of fibrous silica on Y zeolite increased the Lewis acid sites corresponding with the formation of extra-framework Al which led to the generation of more protonic acid sites. A hydrogen adsorbed IR study showed that the protonic acid sites which act as active sites in the isomerization were formed via dissociative-adsorption of molecular hydrogen releasing electrons to the nearby Lewis acid sites. Thus, it is suggested that the presence of Pt and HSi@Y with a high number of Lewis acid as well as weak Bronsted acid sites improved the activity and stability in C_5, C_6 and C_7 isomerization via hydrogen spill-over mechanism.

1. Introduction

There is increasing world demand for the clean gasoline. Due to many restrictions and regulations, it is currently a big challenge for the petroleum refining companies to produce light crude oil with low levels of impurities. World concern related to environmental and health problems has led to regulations that limit the addition of aromatics, benzene, sulfur, NO_x, and other dangerous compounds. Some octane number enhancers such as MTBE and an oxygenated compound have been banned because of alleged leaking from storage tanks and contamination of the water supplies [1]. Also, benzene has been eliminated from gasoline content due to its carcinogenic nature. The restrictions of these compounds in gasoline have affected the gasoline quality and reduced the octane number and thus have contributed to poorer engine performance. In this regard, isomerization processes which convert linear alkanes to higher octane number branched-chain alkanes have been chosen as an alternative way to improve the quality of gasoline [2,3].

The isomerization reaction is generally carried out over bifunctional metal/acidic catalysts consisting of both metallic and acidic functions. In this process, an efficient catalyst is required in order to achieve high selectivity for various isomers and to reduce undesired cracking products. Current industrial catalysts such as platinum supported on halogenated alumina and zirconia have shown good potential for the isomerization reaction. These kinds of catalysts have high activity and selectivity toward *n*-alkane isomers and are able to perform at low reaction temperatures. Platinum has been widely used as a promoter in the production of bifunctional catalysts for isomerization of *n*-alkanes where the metal sites mainly provide the hydrogenation and dehydrogenation function, whereas the acid sites catalyse the isomerization and cracking reactions [4]. It was also reported that Pt has a concomitant role to hydrogenate coke precursors, thus preventing the deposition of carbonaceous over layers [5,6].

However, these catalysts suffer from their complicated operation and they produce serious environmental pollution. Among all of the supports, zeolites, known as microporous crystalline aluminosilicates, are the most promising solid acid catalysts [7,8]. They have been widely used in many industrial processes due to their shape selectivity, good thermal stability, hydrophobicity, and their good ability to transfer electrons to their enormous acid sites. The three-dimensional network with well-defined channels and the

* Corresponding author at: School of Chemical and Energy Engineering, Faculty of Engineering, Universiti Teknologi Malaysia, 81310 UTM Johor Bahru, Johor, Malaysia.
E-mail address: aishahaj@utm.my (A.A. Jalil).

https://doi.org/10.1016/j.jechem.2019.02.016

pore system of zeolites provides high activity and selectivity for the catalytic reactions [9]. Besides, the acidity of the zeolite can be controlled via the Si/Al ratio by using several treatment methods. The amazing properties of zeolites offer new advanced catalytic technologies to produce high-quality products with maximum selectivity and energy efficiency. Unfortunately, zeolites have some diffusion limitations when dealing with bulky compounds owing to their small micropores, which lead to slow mass transport in catalytic reaction processes [10].

Silica-based fibrous material has been extensively studied by researchers after the discovery of the fibrous silica nanosphere (KCC-1) by Polshettiwar and co-workers [11]. The KCC-1 that was prepared using a microwave-assisted hydrothermal technique exhibited excellent properties, including a high surface area, a fibrous surface morphology, good thermal and hydrothermal stabilities, and mechanical stability. Moon et al. reported that mesoporous silica with fibrous morphology has high surface area compared with a typical hexagonal or cubic pore structure which is suitable for a good catalytic support [12]. Previously, numerous studies on acid-catalysed isomerization reactions have been conducted. It has been discovered that the support material for isomerization must have appropriate acidity for good catalytic activity. However, KCC-1, which is fully composed of silica, does not provide an adequate number of acid sites to promote acid-catalysed isomerization reactions [13].

In the present work, a new combined zeolite-based on fibrous silica (HSi@Y) was prepared via self-assembly process in a microemulsion system. This new type of catalyst is supposed to have high and strong acidity due to the presence of extra-framework silica which finally increases the activity and stability of the catalyst.

2. Experimental

2.1. Catalyst preparation

Fibrous silica Y zeolite (Si@Y) was prepared using Y zeolite seed (Zeolyts, CBV 901, Si/Al: 80) crystal-seed crystallization. HSi@Y and Pt/HSi@Y were prepared according to the method described in previous report [14]. In brief, one mole of tetraethyl orthosilicate (TEOS) was dissolved in a mixture of toluene and 1-butanol. Then, the Y zeolite seed was added to the solution followed by stirring for 30 min. A mixed solution of 0.9 moles of urea, 0.27 moles of cetyltrimethyl-ammonium bromide (CTAB) and distilled water was then added. The resulting solution was exposed to intermittent microwave radiation (400 W) for 6 h. The solid product was isolated by centrifugation, followed by washing with acetone and distilled water, and dried overnight in air at 373 K. Finally, the product was calcined at 823 K for 3 h under an air atmosphere. The synthesized catalysts were denoted as fibrous silica Y zeolite (Si@Y).

Pt/HSi@Y was prepared by incipient wetness impregnation of HSi@Y with $H_2PtCl_6{\cdot}6H_2O$ in aqueous solution to obtain 0.5 wt% Pt in the catalyst. The mixture was then stirred and placed in oven until dried and calcined at 823 K for 3 h. The sample was labelled Pt/HSi@Y. For comparison study, the Pt/HY was also prepared.

2.2. Characterization of catalyst

The crystalline structure of catalysts was characterized with X-ray Diffractometer (Bruker Advance D8, 40 kV, 40 mA) using Cu $K\alpha$ radiation with λ= 1.5418 Å radiation in the range of $2\theta = 5°$–90° with a scan rate of 0.1°. The surface morphology was identified using Field Emission Scanning Electron Microscope (FESEM) (Zeiss Supra 35 VP). ^{27}Al and ^{29}Si MAS NMR spectra were determined on a Bruker Advance 400 MHz spectrometer at frequency of 104.2 MHz and 79.4 MHz, respectively. The ^{27}Al MAS NMR spectra were obtained using pulse length of 1.9 μs, spin rate of 7 kHz and relaxation time delay of 2 s. The ^{29}Si MAS NMR spectra were recorded using 4 μs radio frequency pulses, a recycle delay of 60 s and spinning rate of 7 kHz using a 4 mm zirconia. Si/Al ratio of catalysts was determined using Agilent 4100 MP-AES spectrometer. The nitrogen physisorption analysis was done using a Beckman Coulter SA3100. Prior to the measurement, 0.05 g of the catalyst was outgassed at 573 K for 1 h. The adsorption nitrogen was carried out at 77 K. Surface area, pore size distributions and pore volumes were determined from the sorption isotherms using BET and non-local density functional theory (NLDFT) method. Fourier Transform Infra-Red (FTIR) measurements were carried out using Agilent Carry 640 FTIR Spectrometer equipped with a high-temperature stainless steel cell with CaF_2 windows.

Each IR spectrum was measured in transmission mode with a 0.05 g of sample prepared as a self-supported wafer in 13 mm diameter. Prior to IR measurement, the sample was activated at 673 K for 1 h, followed by 2 Torr of pyridine adsorption at 423 K. Then, the pyridine was outgassed at 423, 473, 523, 573 and 623 K. For measurement of the IR spectra for effect of the activation temperature, the catalyst was activated at different temperature of 473, 523, 573, 623 and 673 K. After the activation, it was followed by pyridine adsorption and outgassing at 473 K. In the hydrogen adsorption study, the pyridine pre-adsorbed catalyst was exposed to 100 Torr of hydrogen at room temperature. Then, the catalyst was stepwise-heated from room temperature to 623 K in 50 K increments. All the spectra were recorded on an Agilent Carry 640 FTIR spectrometer [15]. In this study, the amount of adsorbed pyridine was calculated by using integrated molar extinction coefficient (IMEC), 1.67 cm/μmole for Brønsted (B) and 2.2 cm/μmole for Lewis (L) acid sites. The formula involved in the calculation is as follows [14]:

$$C\ (\text{Pyridine on Bronsted acid sites}) = \frac{1.88\ IA(\text{B})R^2}{W} \quad (1)$$

$$C\ (\text{Pyridine on Lewis acid sites}) = \frac{1.42\ IA(\text{L})R^2}{W} \quad (2)$$

where C is the concentration (μmol·cm/g-cat.), IA(B,L) the integrated absorbance of Brønsted or Lewis band, and R is the radius of sample pellet (cm).

2.3. Isomerization of n-alkanes

The isomerization of C_5, C_6 and C_7 was carried out under hydrogen atmosphere in a microcatalytic pulse reactor at temperature range of 423–623 K according to the method described in the previous report [16]. Before the catalytic reaction was performed, 0.3 g of catalyst was subjected to oxygen treatment (F_{Oxygen} = 100 mL/min) for 1 h, followed by hydrogen reduction (F_{Hydrogen} = 100 mL/min) for 3 h at 673 K and cooled down to 548 K in a hydrogen stream. A dose of reactant (14 μmol) was injected over the activated catalyst and the products were trapped at 77 K before flash-evaporation into an online 6090 N Agilent gas chromatograph equipped with HP-5 Capillary Column and FID detector. The intervals between each pulse injection were kept constant at 15 min. Since all catalysts reached steady state condition within 8 pulses (120 min), results at the fourth pulse were used.

The reactant conversion (X_{reactant}), selectivity (S_i) and yield of isomer products (Y_i) were calculated based on th8e following equations:

$$X_{\text{reactant}}(\%) = \frac{\sum [C]_i - [C]_{\text{residual reactant}}}{\sum [C]_i} \times 100\% \quad (3)$$

$$S_i(\%) = \frac{[C]_i}{\sum [C]_i - [C]_{\text{reactant}}} \times 100\% \quad (4)$$

$$Y_i = \frac{X\text{reactant} \times S_i}{100} \quad (5)$$

where $[C]_i$ is a mole number of particular compound. The rate conversion was obtained by multiplication of the differential conversion data and rate constant (k) [17].

3. Results and discussion

3.1. Structural properties

The crystallinity of the catalysts was determined by using XRD analysis. Fig. 1(a) shows XRD patterns of HY, HSi@Y, Pt/HY, and Pt/HSi@Y attributed to the Faujasite-type structure of zeolite Y (JCPDS card 77-1549) for all catalysts at diffraction peaks of $2\theta = 3°–40°$. The typical peaks of the catalysts are well matched with commercial HY and this suggests that the catalysts have the zeolite Y characteristics which can be observed at diffraction peaks of 6.3°, 10.3°, 12.2°, 15.9°, 20.8°, and 24.0° [18]. The introduction of fibrous silica in HY zeolite decreased the crystallinity of HY to about 24%. In particular, a slight shift to the right was observed in HSi@Y compared to HY, suggesting a possible increase of the zeolite unit cell parameter upon the addition of fibrous silica [19]. However, the addition of Pt on HY and HSi@Y did not significantly change the crystallinity of the catalysts. The crystallinity of the catalysts is tabulated in Table 1. The reduction in the intensity of the peaks may be due to the collapsing of the aluminosilicate framework and/or to the formation of an excessive amount of silicate extra-framework upon the addition of fibrous silica. Another study revealed that there is a partial collapse of the FAU structure in USY after steam treatment at 925 °C [20]. Sun et al. reported that modification of zeolite Y (which has the structure of KF-Y) with potassium completely collapsed the zeolite Y after activation and reflected the transformation of zeolite to amorphous aluminosilicate [18]. In the other study, the intensity of XRD for PtY was reduced compared to commercial NaY because of interference effects from the Pt ions impregnated into the zeolite [21]. In contrast, the introduction of iridium into Fe-USY did not change the XRD pattern of Fe-USY because of the well-controlled deposition of iridium onto Fe-USY [22].

Fig. 1(b) shows an FESEM image of the spherical fibrous morphology of Pt/HSi@Y. The Pt/HSi@Y exhibited bicontinuous lamellar growth radially outward from the zeolite core which arranged in three dimensions to form a colloidal sphere shape with open pore channels. This unique fibrous silica morphology mimicked the KCC-1 proposed by Polshettiwar et al. [11]. The KCC-1 was suggested to have several advantages such as a high surface area to provide high accessibility for the bulky mass reactants to access active sites and this increases the rate of reaction and product formation [12]. The particle size distribution of Pt/HSi@Y is in the range of 500–700 nm (Fig. 1c). Upon the introduction of Pt, there were no significant changes in morphology or particle size of HSi@Y. The EDX analysis revealed that the catalysts were composed of Si, Al, and O atoms. The addition of Si species from hydrolysis of TEOS by urea resulted in an increase in the amount of Si on Pt/HSi@Y catalyst from 85.5 wt% to 94.0 wt%. It can be claimed that Pt/HSi@Y possesses dendrimeric silica fibres which are arranged in three dimensions to form a sphere. This result is supported by the Si/Al ratio obtained with MPAES in which the Pt/HSi@Y type catalysts possessed a higher Si/Al ratio as compared to commercial Pt/HY. The Si/Al ratio of Pt/HSi@Y increased from 41 to 110 (Table 1).

The ^{27}Al MAS NMR analysis was carried out to detect the presence of a tetrahedral framework for aluminium (isolated AlO_4 species) and an octahedral extra-framework aluminium (AlOH species) [23]. Fig. 2 shows a typical aluminium spectrum with two distinctive peaks at 54 and 0 ppm, which are attributed to

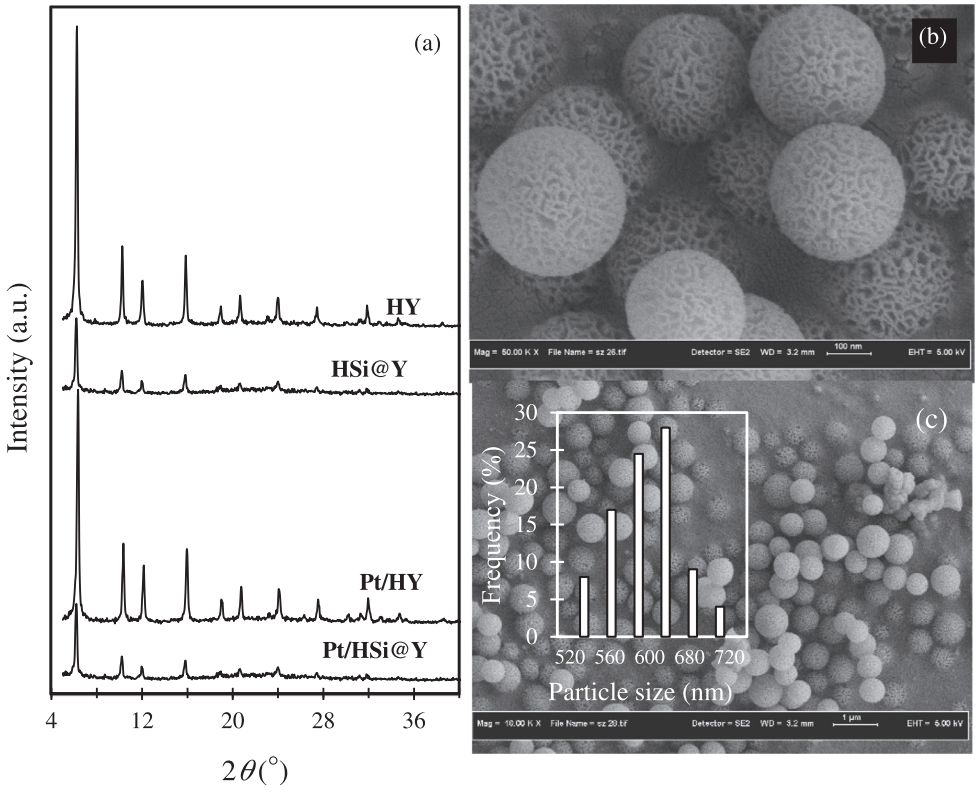

Fig. 1. (a) XRD patterns of all catalysts and, (b) FESEM images and (c) particles size distribution of Pt/HSi@Y.

Table 1. Physicochemical properties of catalysts.

Catalysts	Si/Al ratio[a]	Crystallinity[b] (%)	Surface area[c] (m^2/g)	Mesopore volume[d] (cm^3/g)	Total pore volume[d] (cm^3/g)	Bronsted acid site[e] (μmol/g-cat)	Lewis acid site[e] (μmol/g-cat)
HY	42	100	473	0.044	0.308	9.64	8.96
HSi@Y	108	24	550	0.710	0.808	6.08	13.84
Pt/HY	41	78	466	0.035	0.299	11.50(0.015)[f]	7.49
Pt/HSi@Y	110	24	483	0.518	0.604	5.16(0.037)[f]	15.34

[a] Obtained by Microwave Plasma Atomic Emission Spectroscopy (MPAES).
[b] The intensity ratio was used to determine the crystallinity of the catalysts and assumed that the crystallinity of HY is 100% at peak intensity at $2\theta = 6.3°$.
[c] BET method.
[d] Mesopore and total pore volume were obtained from *t*-plot method.
[e] The amount of Bronsted and Lewis acid sites was calculated using the integrated molar extinction coefficients for which $\varepsilon 1546 = 1.67$ cm μmol^{-1} for the Bronsted and $\varepsilon 1446 = 2.22$ cm μmol^{-1} for the Lewis acid sites.
[f] The catalysts were outgassed at 623 K.

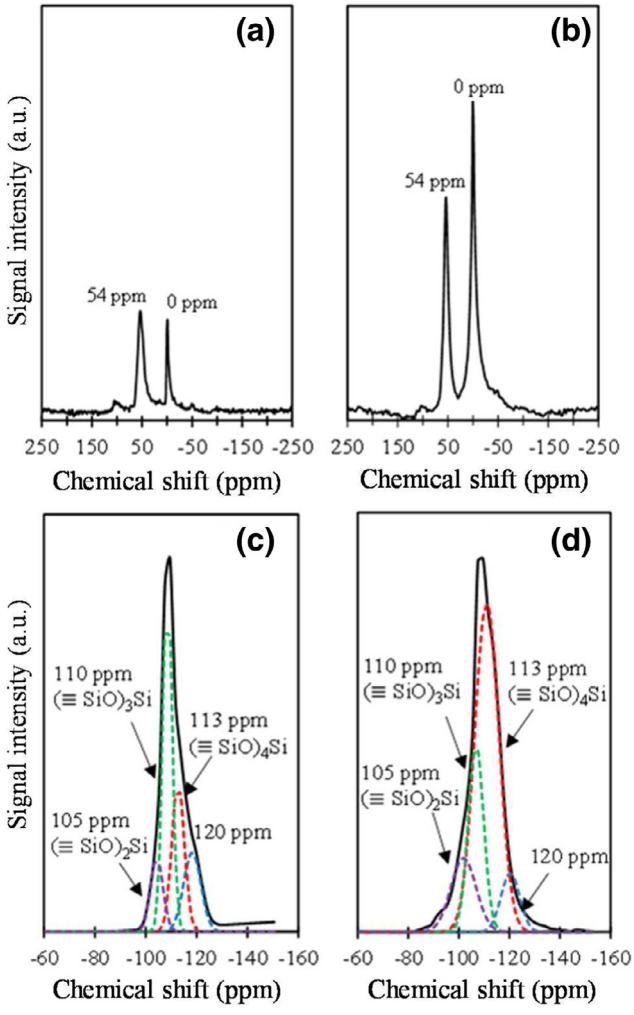

Fig. 2. ^{27}Al (a: Pt/HY; b: Pt/HSi@Y) and ^{29}Si (c: Pt/HY; d: Pt/HSi@Y) MAS NMR spectra of all catalysts.

the tetrahedrally and octahedrally-coordinated aluminium, respectively [24]. The ratio of extra-framework/framework aluminium for Pt/HY and Pt/HSi@Y were 0.98 and 1.39, respectively. The higher ratio for Pt/HSi@Y indicated collapsing of the tetrahedral coordinated framework aluminium.

From the ^{29}Si MAS NMR, Pt/HY exhibited a dominant signal at −110 ppm that was attributed to Q_3 site, $(\equiv SiO)_3Si$. While, Pt/HSi@Y exhibited one dominant signal at −113 ppm which corresponds to silicon atoms at Q_4 sites, $(\equiv SiO)_4Si$. Also, a small peak was observed at −105 ppm both for Pt/HY and Pt/HSi@Y. This corresponds to Q_2 site, $(\equiv SiO)_2Si$. Both Pt/HY and Pt/HSi@Y possessed an inequivalent crystallography site at −120 ppm [25]. The dominant Q_4 sites at Pt/HSi@Y indicated that the addition of dendrimeric silica fibre increased the amount of Q_4 silicate framework. Gore, et al. reported that increasing the Si/Al ratio of USY zeolite showed regularly ordered Q_4 (Si) framework sites at approximately −105 ppm and loss of Si (3Si, 1Al) and Si (2Si, 2Al) environments [8]. This result corresponds to the Si/Al ratio obtained from MPAES in which the Si/Al ratio increased from 41 to 110.

According to XRD, NMR, and FESEM results, it can be concluded that Pt/HSi@Y was predominantly composed of silica and small part of the HY framework. The centre of Pt/HSi@Y consists of HY and on the outer part (dendrimer) was mainly composed of silica. This phenomenon mimics our previous report where elemental mapping showed that the aluminosilicate framework of ZSM-5 was at the centre of the Pt/HFZSM-5 sphere and the silica was mainly distributed at the outer part of the Pt/HFZSM-5 sphere [14].

The N_2 adsorption-desorption isotherms and pore size distributions for all catalysts are plotted in Fig. 3. All catalysts showed a nitrogen uptake at a low relative pressure, which is due to the presence of microporosity. Two up-steps can be observed at $P/P_0 = 0.5$ and 0.9 for HSi@Y type catalysts, indicating the presence of capillary condensation of nitrogen in the intraparticle and interparticle voids, respectively. Higher nitrogen uptake was revealed in HSi@Y type catalysts, suggesting the presence of mesopores. The HSi@Y type catalysts showed type IV adsorption isotherms with an H_3 hysteresis loop, indicating the presence of mesopores with non-uniform slit-shaped pores. It was clearly observed that the introduction of fibrous silica in HY resulted in the presence of porous material consisting of micropores and mesopores. Meanwhile, commercial HY type catalysts showed type I isotherms. HY type catalysts showed high nitrogen uptake at low relative pressure and relatively low nitrogen uptake at high relative pressure; this indicates that only micropores are present [26]. In addition, all catalysts showed bimodal pore size distributions in which narrow peaks were observed in the range of 1–2 nm and 3–6 nm. These were attributed to micropores and mesopores, respectively. A peak observed in the range of 1–2 nm for HY showed that the catalyst was dominated by micropores. The addition of fibrous silica increased the peak in the range of 3–6 nm which indicated that the mesopores were formed from the self-assembly of the CTAB surfactant and the inter-dendrimer distance in HSi@Y catalyst. It was observed that the peak at 3–6 nm on Pt/HSi@Y was slightly decreased. This may be due to a change of crystallinity which is in accordance with the XRD results. Other than that, it also may be due to a blocked entrance to the porous network or to occupied inner pores of the catalyst which resulted from the impregnation by Pt metal.

From the Table 1, HSi@Y exhibited a slightly higher surface area (550 m^2/g) as compared to HY (473 m^2/g). The total pore volume of HSi@Y is 0.808 cm^3/g, which shows that HSi@Y possesses more

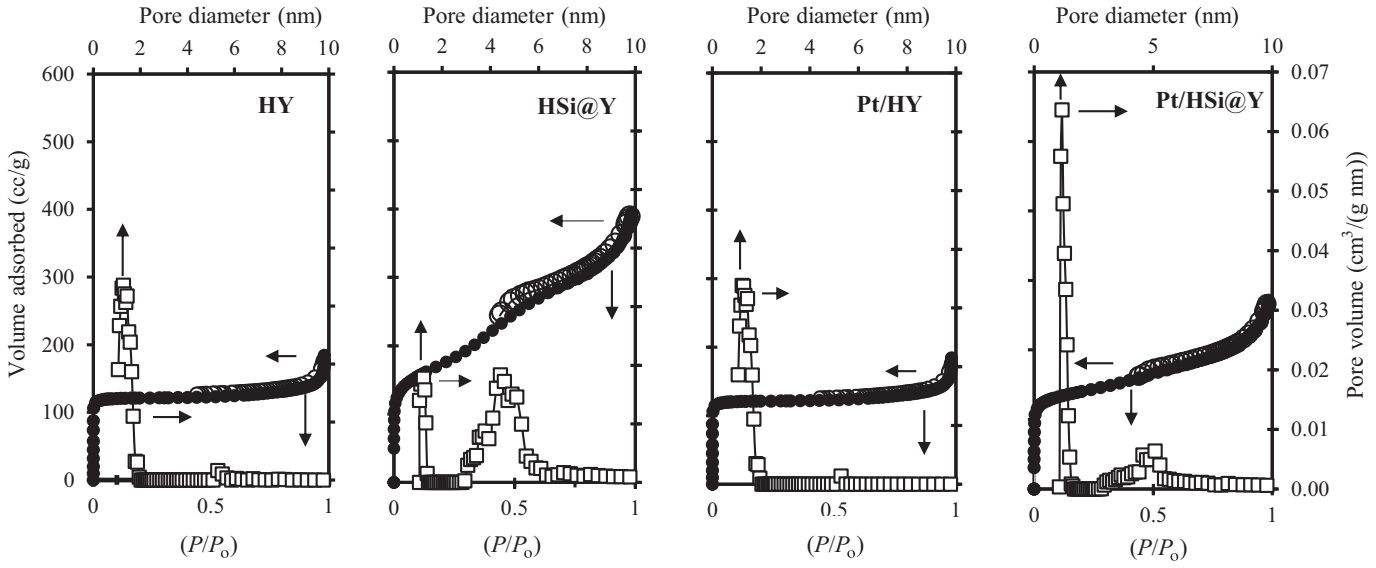

Fig. 3. N_2 adsorption (white-circle symbol)-desorption (black-circle symbol) isotherms and NLDFT pore size distribution of all catalysts.

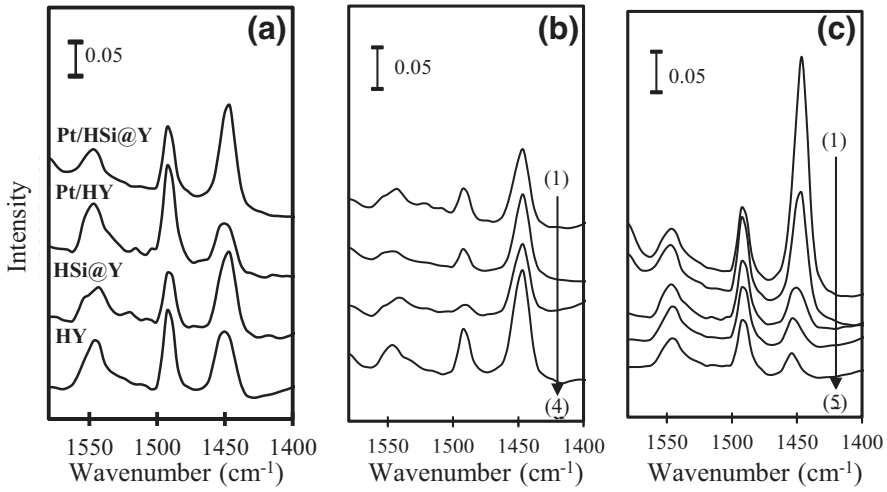

Fig. 4. (a) IR spectra of pyridine adsorbed on all catalysts. The catalyst was activated at 673 K, followed by pyridine adsorption at 423 K and outgassing at 473 K. (b) IR spectra of pyridine adsorbed on Pt/HSi@Y when the catalyst was activated at different temperature (1) 523 K, (2) 573 K, (3) 623 K, and (4) 673 K. (c) IR spectra of pyridine adsorbed on Pt/HSi@Y at 423 K followed by outgassing at (1) 423 K, (2) 473 K, (3) 523 K, (4) 573 K, and (5) 623 K.

mesopore and micropore volume than HY (0.308 cm^3/g). The increase in the BET surface area of HSi@Y type catalysts may be due to the formation of dendrimeric silica upon the addition of silica to the parent HY. The increase in the amount of mesopores from 0.044 to 0.710 cm^3/g was suggested to be due to the formation of mesopores in dendrimeric silica. In addition, the amount of micropore volume was slightly decreased, which might be due to blockage by the presence of the silicate framework. In this study, the introduction of Pt into HSi@Y and HY has slightly decreased the surface area and total pore volume. This result may be due to blockage of the entrances to the porous network or to occupation of the inner pores of the catalysts by Pt particles [14].

3.2. IR study of pyridine adsorption

The type of acid sites for HY, HSi@Y, Pt/HY and Pt/HSi@Y was studied by pyridine adsorbed IR spectroscopy. Fig. 4(a) shows IR bands for all activated catalysts in which the pyridine was adsorbed at 423 K until equilibrium and outgassed at 473 K. All of the catalysts exhibited two absorbance bands at 1454 and 1545 cm^{-1}, which are attributed to pyridine molecules coordinated to Lewis acid sites and to pyridinium ions formed by protonation of pyridine on Brønsted acid sites, respectively [4]. Besides, another band was observed at 1490 cm^{-1}, which corresponded to the conjugation of Brønsted and Lewis acid sites. In particular, the HSi@Y type catalysts possessed higher peak intensity of Lewis acid sites compared to the HY type catalysts (Fig. 4a), which was possibly due to the generation of extra-framework Al sites during the synthesis procedure using water as solvent. This result is in agreement with the ^{27}Al MAS NMR spectroscopy which showed an increase in extra-framework Al in Pt/HSi@Y compared to the Pt/HY. Besides, this result was also in accordance with the change of a peak in OH region, as observed by FTIR spectra of evacuated catalyst at 673 K (Fig. S2). Deconvolution spectrum by Gaussian curve-fitting of Pt/HSi@Y exhibited a higher peak at 3660 cm^{-1} which corresponded to extra-framework Al-OH species compared to the Pt/HY. Similar results have been reported by Katada et al. who showed that water treatment on a series of ultra-stable Y zeolites resulted in higher formation of extra-framework aluminium [27].

Fig. 4(b) shows IR spectra for Pt/HSi@Y at different activation temperatures from 523 K to 673 K and pyridine was adsorbed at 423 K. As the activation temperature was raised, the Lewis acid sites increased while the Brønsted acid sites decreased. The intensity ratio of Lewis to Brønsted increased markedly with increasing the activation temperature. This phenomenon was due to the dehydration and/or dihydroxylation which eliminated acidic OH groups at higher activation temperatures [28]. In addition, a high number of Lewis acid sites in Pt/HSi@Y represented the perturbed framework Al atoms in which Lewis acid sites formed from the partial zeolite dehydroxylation in the presence of extra-framework Al in which most of the Lewis acid sites have origin in the extra-framework Al atoms [29]. This result was evidenced by the ^{27}Al NMR result, which showed that the signal intensity of extra-framework AlOH species (Lewis acid sites) in the super-cages and sodalite cages is higher for HSi@Y than HY [30]. A decrease in Brønsted acidity and an increase in Lewis acidity in high silica HZSM-5 was reported to be due to the transformation of part of the four-coordinated framework Al atoms into six-coordinated extra-framework atoms [31]. Upon the introduction of Pt on both HY and HSi@Y, only slight changes occur in the Lewis and Brønsted acid sites which means that Pt did not significantly affect the acidity. Fig. 4(c) shows IR spectra for Pt/HSi@Y outgassing of pyridine at elevated temperatures from 423 to 623 K. Upon increasing the outgassing temperature, pyridine molecules adsorbed on weak acid sites will be desorbed at lower temperatures and pyridine molecules adsorbed on strong acid sites will be desorbed at higher temperatures [16]. The results showed that all types of catalysts possessed Lewis and Brønsted acid sites after outgassing of adsorbed pyridine at 573 K. This indicates that Pt/HSi@Y type catalysts possess relatively weak and strong acid sites [32].

3.3. C_5–C_7 isomerization

The catalytic activities of HY, HSi@Y, Pt/HY, and Pt/HSi@Y were evaluated with respect to C_5, C_6 and C_7 isomerization at 423–623 K in a microcatalytic pulse reactor in the presence of hydrogen gas (Figs. 5 and 6). Prior to the reaction, all catalysts were activated at 673 K under a hydrogen stream for 3 h. For all reaction temperatures, HY and HSi@Y were not active for C_5, C_6 and C_7 isomerization. This may be due to the absence of active sites for initiation of the reaction. The presence of a Pt site enhanced the activity of the catalysts. Fig. 5 shows the rate conversion and yield of isomers for C_5, C_6, and C_7 isomerizations over Pt/HY and Pt/HSi@Y, while their respective selectivity towards isomers and cracking are illustrated in Fig. 6. Although, the results showed that Pt/HSi@Y gives better activity than that of Pt/HY, in general both catalysts showed poor activity for C_5 isomerization at all temperatures compared with C_6 and C_7 isomerizations. Both catalysts yielded less than 3% of mono branched-isomer product and no di-branched isomers were detected. The rate of reaction was higher with Pt/HSi@Y for C_5 and C_6 isomerizations. Particularly, the rate of C_6 isomerization reached almost three-times higher for Pt/HSi@Y. Similarly, the yield of isomers was higher for Pt/HSi@Y than that for Pt/HY. The yield for C_5, C_6 and C_7 isomerization was less than 22% for Pt/HY. For Pt/HSi@Y, the yield of isomers for C_6 and C_7 isomerizations reached 70% and 30% at 623 K. Above 573 K, although the rate of reaction increased, the yield of C_7 isomerization did not change much. This may be due to the formation of cracking products at higher reaction temperatures. The high activity in terms of isomer yield over Pt/HSi@Y was possibly due to the presence of a moderate amount of weak Bronsted acid sites, which originated from the fibrous silica framework. This result is in accordance with the results observed in pyridine FTIR with different activation temperatures (Fig. 4) which showed that Pt/HSi@Y possessed weaker Bronsted acid sites compared to Pt/HY. The moderate amount of weak Bronsted acid sites

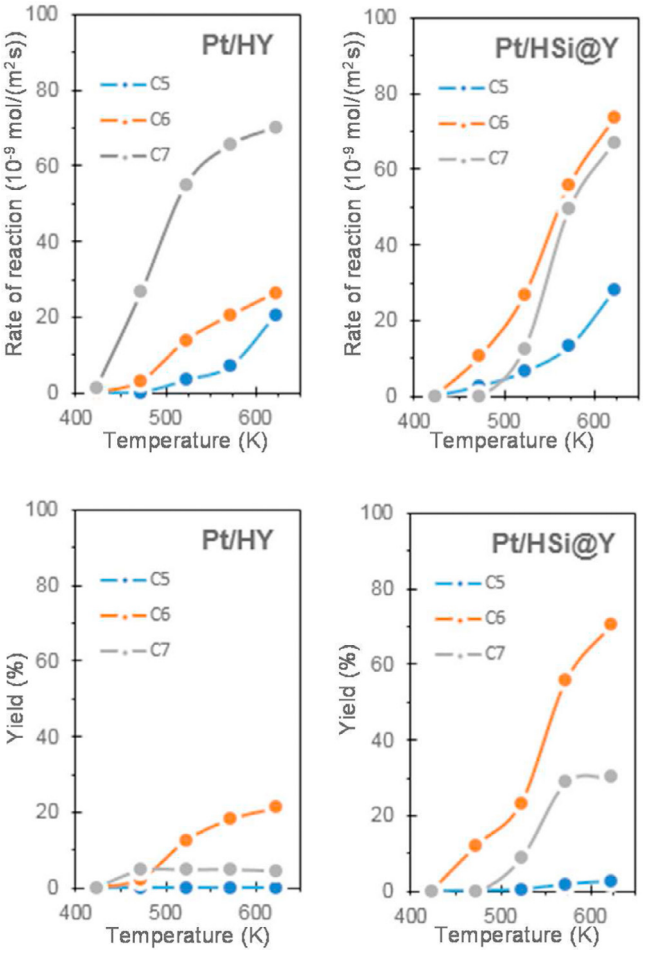

Fig. 5. Rate conversion and yield isomer products for isomerization of C_5, C_6 and C_7 at different reaction temperatures over Pt/HY and Pt/HSi@Y.

enhanced the yield of isomers by forming bigger cracking products of C_5–C_6 (as tabulated in Table S1) which can further rearrange to form isomer products. Meanwhile, the strong Bronsted acid sites in Pt/HY favours the formation of smaller C_1–C_2 cracking products, which subsequently decreased the yield of isomers.

On the other hand, Pt/HY and Pt/HSi@Y showed a better rate of conversion and produced mono and di-branched isomers compared with Pt-free catalysts. This is due to the fact that the Pt site provided a metallic-acid balance function to convert the alkane reactants into isomer products. Moreover, the Pt has a role in the formation of protonic acid sites through a hydrogen spill-over phenomenon which finally promoted the isomerization [4,9]. The presence of metallic platinum dissociates hydrogen molecules to hydrogen atoms which undergo spill-over over on the support. The dissociated hydrogen molecules are not only indispensable for the generation of the acid sites, but also inhibit the formation of ß-scission that is responsible for cracking and polymerization reactions by eliminating the ionic intermediates from the catalyst surface. Furthermore, the catalyst with Pt was suggested to have fewer cracking products than the Pt-free catalysts. This was evident from the study of Santikunapom et al. in which Pt/HY produced lower amounts of cracking products and enhanced the stability of the catalyst in the ring opening reaction of decalin and tetralin [33].

In this study, Pt/HSi@Y possessed higher catalytic activity than Pt/HY and most probably this was correlated to the addition of fibrous silica into the catalyst surface. The addition of silica was suggested to produce a higher amount of Lewis acid sites which assist

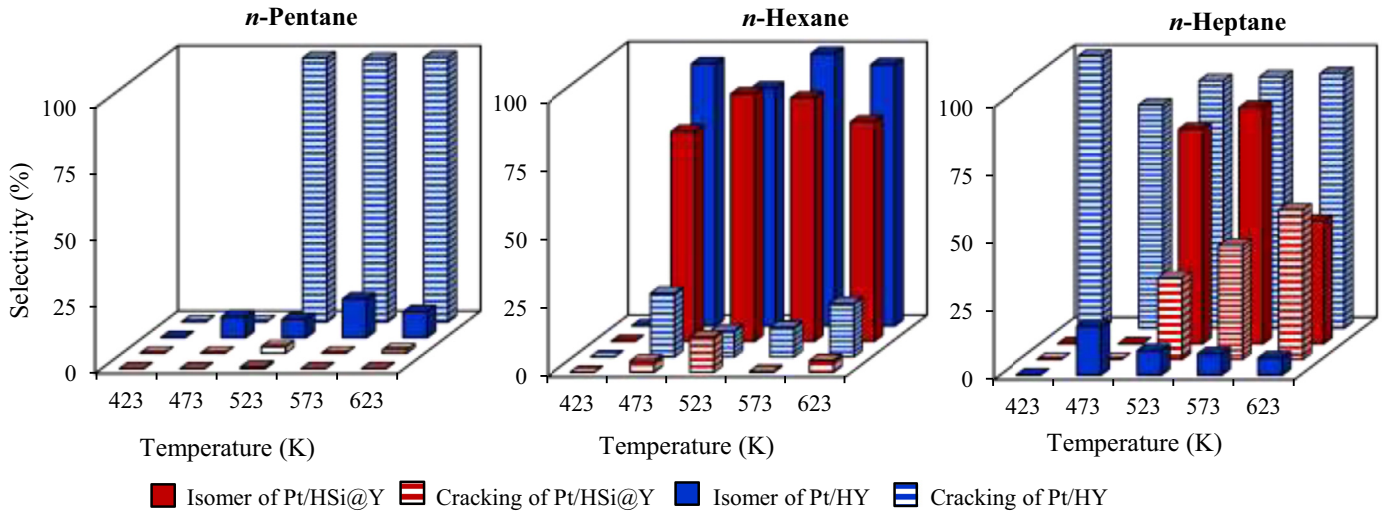

Fig. 6. Product selectivity of *n*-pentane, *n*-hexane and *n*-heptane isomerization isomerization over Pt/HY and Pt/HSi@Y in the presence of hydrogen.

in the generation of protonic acid sites from molecular hydrogen. It is noteworthy that the formation of protonic acid sites originated from molecular hydrogen atoms releasing electrons. Then, the electrons may react with a second hydrogen atom to form a hydride or they are stabilized in the Lewis acid sites. Moreover, a slight increase in the total acidity was observed after the introduction of Pt in both HY and HSi@Y catalysts. The increase in the total acidity in the presence of Pt was plausibly attributed to an enhancement of the dehydroxylation or dehydration process which leaves Lewis acid sites. Also, similar results were observed in a previous report on MoO_3 catalyst which showed an increase in acidity after the addition of Pt due to the elimination of OH groups [34].

The formation of protonic acid sites was evident by the pyridine-pre-adsorbed IR heated in hydrogen at elevated temperature as shown in Fig. 7. By increasing the temperature in the presence of hydrogen, the absorbance intensity of the band at 1445 cm^{-1} (Lewis acid sites) decreased with a concomitant increase in the absorbance intensity at the 1545 cm^{-1} (protonic acid sites) band. This indicated that the formation of protonic acid sites was through interconversion of the Lewis acid sites to protonic acid sites. The formation of protonic acid sites for Pt/HSi@Y was higher than for Pt/HY. The change of protonic acid site intensity for Pt/HSi@Y was 0.037 where only 0.015 was produced for Pt/HY. The high ability of the Pt/HSi@Y catalyst to generate protonic acid sites may correspond to the surface changes brought about in the formation of the extra-framework upon the introduction of fibrous silica onto the Pt/HY, which results in an increased amount of Lewis acid sites as electron acceptors. It should be noted that formation of protonic acid sites from molecular hydrogen in Pt/HSi@Y corresponded to the large amount of Lewis acid sites from the presence of fibrous silica and the presence of Pt [35]. According to Prins et al., the spill-over of hydrogen can occur in the presence of defect sites on the catalysts in which O^- on the surface and holes trapped in a cation vacancy can dissociate H_2 and form OH^- ions [36]. The presence of Pt in the catalyst was essential for the catalyst to facilitate the formation of protonic acid sites from molecular hydrogen [37]. As compared with Pt/HY, Pt/HSi@Y showed a greater change in the absorbance band and this indicated that the fibrous silica catalyst has facilitated the formation of protonic acid sites. We also reported that the conversion of Lewis acid sites into protonic acid sites on Pt/WO_3-ZrO_2 occurred at lower temperatures compared to WO_3-ZrO_2, which indicated that the rate of protonic acid sites formation is higher in a catalyst with Pt than without Pt [4]. In addition, the presence of Pt enhanced the production rate of

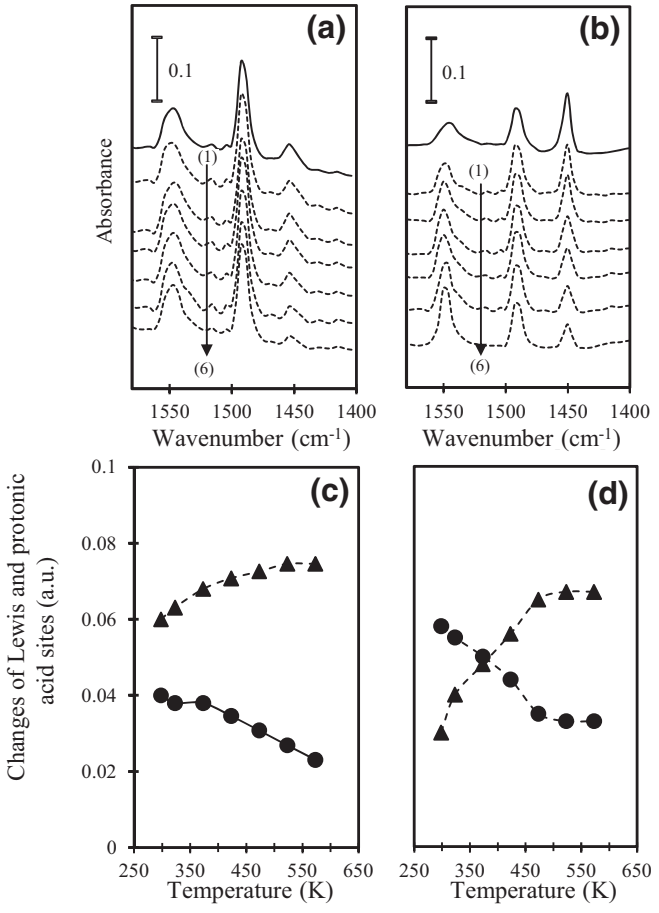

Fig. 7. (a,b) Spectral changes of all catalysts when pyridine-preadsorbed sample was heated in hydrogen at (1) RT, (2) 323 K, (3) 373 K, (4) 423 K, (5) 473 K and (6) 523 K. Pyridine outgassed at 623 K (solid line). (c,d) Variations of the absorbance intensity for the spectral changes when pyridine-preadsorbed sample was heated in hydrogen. Lewis acid sites (●) and protonic acid sites (▲).

protonic acid sites from the hydrogen spill-over mechanism. This phenomenon has also been observed on Pt/SO_4^{2-}-ZrO_2 catalyst by Hattori et al. [38]. They concluded that hydrogen molecules were dissociatively adsorbed on the Pt to form a proton and a

Table 2. Comparison study for C_5–C_7 isomerization.

Reactant	Catalyst	Conversion (%)	S_{iso} (%)		*S* cracking (%)	Yield isoproducts (%)	Reaction temperature (K)	Ref.
			Mono-branched	Di-branched				
C_7	Pt/HSi@Y	87.4	75.0	2.5	22.5	67.7	623	This study
	Pt/HY	92.3	14.6	–	83.9	13.3	623	This study
	Pt/Hβ	71.8	70.1	23.9	6	67.5	453	[1]
	MoO_3/MSN	45	81.3	12.4	3.5	43.4	623	[17]
C_6	Pt/HSi@Y	72.3	91.4	7.7	5.7	71.7	573	This study
	Pt/HY	27.2	70.7	1.7	27.4	19.5	573	This study
	Pt/HMOR	24.0	74.7	15.8	–	21.7	523	[39]
	Pt/WO_x-ZrO_2	39.0	86.8	12.6	–	38.8	533	[42]
	MoO_3/TiO_2	34.5	81.8	10.0	–	31.7	573	[43]
C_5	Pt/HSi@Y	60.3	45.0	8.5	6.5	53.5	623	This study
	Pt/HY	22.7	10.3	4.6	6.1	3.4	623	This study
	Zn/Hβ	29.7	75.0	–	25.0	22.3	623	[8]
	Ir/Pt-HZSM5	63.0	98.2	–	–	57.2	548	[32]

hydride ion. The proton was present as spill-over hydrogen and the hydride ion was trapped on the Lewis acid site. Other research found that the elimination of protonic acid sites and the formation of strong Lewis acid sites on HZSM5 may be caused by the existence of metal species bonded to the non-acidic terminal (SiOH) group and/or the bridging hydroxyl (SiOHAl) groups on the surface of HZSM5 [9]. Monteiro et al. studied the catalytic behaviour of Pt/HMOR in *n*-hexane hydro-isomerization by the modification of zeolite pores [39]. They concluded that the selectivity of di-branched isomers was improved due to the preservation of the support acidity and the slight enlargement of the micropores. This work was similar to Pt/HSi@Y where the modification of HY to HSi@Y enlarged the pores size for better performance in catalytic activity. In this study, the role of mesopores in enhancement of catalytic performance can be determined by examining the difference in product distribution obtained over HY and HSi@Y based catalysts as presented in Table 2. The presence of mesopores in Pt/HSi@Y has facilitated the formation of bigger size di-branched isomer products which have higher RON in C_6 isomerization. At reaction temperatures of 523–623 K, it was observed that Pt/HSi@Y gave 15.91% selectivity of 2,3-DMB compared to 11.3% over Pt/HY.

Table 2 shows the catalytic activity of catalysts for C_5–C_7 isomerizations reported in literature. It is observed that non-zeolite catalysts such as MoO_3/MSN showed high activity and stability in C_7 isomerization at 623 K. This was due to the dissociative-adsorption of molecular hydrogen on MoO_3 to form atomic hydrogen, which consequently enhanced the formation of protonic acid sites [17]. Meanwhile, Monteiro et al. enhanced the activity of C_6 hydro-isomerization over Pt/HMOR by controlling the support acidity and the size of the micropores [39]. Besides, Katrib et al. revealed that the reduction of bifunctional MoO_3/TiO_2 formed a $MoO_2(H_x)$ac phase which provided hydrogenation and dehydrogenation sites for enhanced C_6 isomerization [40]. It was also found that Zn loading on Hβ showed good activity in C_5 isomerization due to the presence of strong Lewis acid sites which facilitate the formation of active protonic acid sites through a hydrogen spill-over mechanism [8]. Setiabudi et al. studied the effect of iridium (Ir) loading on Pt-HZSM-5 for C_5 isomerization [41]. It was found that the Ir enhanced the selectivity for iso-pentane and decreased the selectivity for cracking products due to the interaction of iridium with lattice defects or with extra-lattice oxygen that increased the number of strong Lewis and protonic acid sites from molecular hydrogen. It is noteworthy that the results of Pt/HSi@Y are up to par compared to the other above-mentioned catalysts, particularly for the C_7 and C_6 isomerization. This certainly due to the presence of dendrimeric fibre on Pt/HSi@Y which contributed to the abundance of Lewis acid sites. Meanwhile, slightly lower activity of C_5 isomerization was observed which might be attributed to the dehydroisomerization and hydrocracking of C_5. In fact, C_5 with only a five carbon chain is more challenging for isomerization as compared to C_6 and C_7.

4. Conclusions

Fibrous Y (Si@Y) zeolite was successfully prepared using bi-continuous microemulsion of CTAB, toluene, and water coupled with zeolite crystal-seed crystallization. While, Pt/HSi@Y and Pt/HY have been prepared by protonation of Si@Y and commercial Y followed by impregnation with platinum. All of the catalysts were characterized using XRD, FESEM-EDX, NMR, N_2 physisorption, and FTIR spectroscopy. XRD results showed that the HSi@Y pattern is well matched with the HY pattern which indicated that the framework structure of zeolite is unaltered during the introduction of fibrous silica into the zeolite Y. FESEM images showed the bi-continuous lamellar morphology of Pt/HSi@Y in which HY acts as a core and the fibrous silica as a shell and EDX indicated that silica is the dominant component in the Pt/HSi@Y type catalyst. This result correlated with the NMR result in which the Pt/HSi@Y possessed a high extra-framework to framework ratio which indicated that Pt/HSi@Y possessed a dominant amount of Q_4 site. The N_2 physisorption of Pt/HSi@Y exhibited type IV isotherms with H_3 hysteresis which indicated the presence of mesopores with a high BET surface area and pore volume. In general, the activity of Pt/HSi@Y was better than Pt/HY, HSi@Y, and HY catalysts for C_5, C_6 and C_7 isomerizations at 423–623 K. Particularly, Pt/HSi@Y showed better activity for C_6 and C_7 isomerizations at 473–623 K.

The high activity of Pt/HSi@Y was attributed to the presence of weak Bronsted acid sites that originated from the silica framework in the fibrous silica. This enhanced the formation of isomer products, while suppressing the selectivity towards cracking products. Meanwhile, the presence of a high number of Lewis acid sites from the extra-framework aluminium facilitates the generation of protonic acid sites from molecular hydrogen. The generation of protonic acid was initiated from hydrogen spill-over molecules on the catalyst surface which produced electrons captured by Lewis acid sites. From these results, it was concluded that Pt/HSi@Y is a versatile catalyst for generating protonic acid sites due to the presence of more Lewis acid sites as well as weak Bronsted acid sites. Therefore, fibrous silica catalysts were proven to have an appropriate acidic property to obtain high performance in light alkane isomerization.

Acknowledgments

This work was supported by the Universiti Teknologi Malaysia through Research University Grant No. 13H61 and 19H04. Our gratitude also goes to the Ministry of Higher Education Malaysia for the award of MyMaster Scholarship.

Supplementary material

Supplementary material associated with this article can be found, in the online version, at doi:10.1016/j.jechem.2019.02.016.

References

[1] V.M. Akhmedov, S.H. Al-Khowaiter, Catal. Rev. 49 (2007) 33–139.
[2] M. Busto, L.A. Dosso, C.R. Vera, J.M. Grau, Fuel Process. Technol. 104 (2012) 128–135.
[3] X. Zhu, Y. Wang, X. Li, H. Li, P. Zeng, J. An, F. Chen, S. Xie, H. Lan, D. Wang, S. Liu, L. Xu, J. Energy Chem. 22 (2013) 755–760.
[4] S. Triwahyono, T. Yamada, H. Hattori, Appl. Catal. A Gen. 242 (2003) 101–109.
[5] M.J. Wulfers, G. Tzolova-Müller, J.I. Villegas, D.Y. Murzin, F.C. Jentoft, J. Catal. 296 (2012) 132–142.
[6] P. Wang, J. Zhang, G. Wang, C. Li, C. Yang, J. Catal. 338 (2016) 124–134.
[7] Z. Yang, J. Li, Y. Liu, C. Liu, J. Energy Chem. 26 (2017) 688–694.
[8] N.H.N. Kamarudin, A.A. Jalil, S. Triwahyono, R.R. Mukti, M.A.A. Aziz, H.D. Setiabudi, M.N.M. Muhid, H. Hamdan, Appl. Catal. A Gen. 431–432 (2012) 104–112.
[9] H.D. Setiabudi, A.A. Jalil, S. Triwahyono, N.H.N. Kamarudin, R.R. Mukti, Appl. Catal. A Gen. 417–418 (2012) 190–199.
[10] M. Zhang, L. Wang, Y. Chen, Q. Zhang, C. Liang, J. Energy Chem. 25 (2016) 539–544.
[11] V. Polshettiwar, D. Cha, X. Zhang, J.M. Basset, Angew. Chemie - Int. Ed. 49 (2010) 9652–9656.
[12] D.-S. Moon, J.-K. Lee, Langmuir 28 (2012) 12341–12347.
[13] N.A.A. Fatah, S. Triwahyono, A.A. Jalil, N. Salamun, C.R. Mamat, Z.A. Majid, Chem. Eng. J. 314 (2017) 650–659.
[14] M.L. Firmansyah, A.A. Jalil, S. Triwahyono, H. Hamdan, M.M. Salleh, W.F.W. Ahmad, G.T.M. Kadja, Catal. Sci. Technol. 6 (2016) 5178–5182.
[15] S. Triwahyono, T. Yamada, H. Hattori, Appl. Catal. A Gen. 250 (2003) 75–81.
[16] S. Triwahyono, A.A. Jalil, N.N. Ruslan, H.D. Setiabudi, N.H.N. Kamarudin, J. Catal. 303 (2013) 50–59.
[17] N. Fatah, S. Triwahyono, A. Jalil, A. Ahmad, T. Abdullah, Appl. Catal. A Gen. 516 (2016) 135–143.
[18] L.B. Sun, L. Gong, X.Q. Liu, F.N. Gu, Y. Chun, J.H. Zhu, Catal. Lett. 132 (2009) 218–224.
[19] M. Richter, M.J.G. Fait, R. Eckelt, M. Schneider, J. Radnik, D. Heidemann, R. Fricke, J. Catal. 245 (2007) 11–24.
[20] K.U. Gore, A. Abraham, S.G. Hegde, R. Kumar, J. Amoureux, S. Ganapathy, J. Phys. Chem. B 106 (2002) 6115–6120.
[21] Y. Yang, L. Bourgeois, C. Zhao, D. Zhao, A. Chaffee, P.A. Webley, Microporous Mesoporous Mater. 119 (2009) 39–46.
[22] S. Li, S. Huang, W. Shen, H. Zhang, H. Fang, A. Zheng, S. Liu, F. Deng, J. Phys. Chem. C. 112 (2008) 14486–14494.
[23] Y. Fang, X. Su, X. Bai, W. Wu, G. Wang, L. Xiao, A. Yu, J. Energy Chem. 26 (2017) 768–775.
[24] L.P. Teh, S. Triwahyono, A.A. Jalil, R.R. Mukti, M.A.A. Aziz, T. Shishido, Chem. Eng. J. 270 (2015) 196–204.
[25] G. Engelhardt, U. Lohse, Zeolites 2 (1982) 59–62.
[26] S. Jin, Z. Xiao, C. Li, C.T. Williams, C. Liang, J. Energy Chem. 23 (2014) 185–192.
[27] N. Katada, Y. Kageyama, K. Takahara, T. Kanai, H. Ara Begum, M. Niwa, J. Mol. Catal. A Chem. 211 (2004) 119–130.
[28] S.N. Timmiati, A.A. Jalil, S. Triwahyono, H.D. Setiabudi, N.H.R. Annuar, Appl. Catal. A Gen. 459 (2013) 8–16.
[29] K. Tarach, K. Góra-marek, J. Tekla, K. Brylewska, J. Datka, K. Mlekodaj, W. Makowski, J. Catal. 312 (2014) 46–57.
[30] J.N. Kondo, R. Nishitani, E. Yoda, T. Yokoi, T. Tatsumi, K. Domen, Phys. Chem. Chem. Phys. 12 (2010) 11576–11586.
[31] C. Mei, P. Wen, Z. Liu, H. Liu, Y. Wang, W. Yang, Z. Xie, W. Hua, Z. Gao, J. Catal. 258 (2008) 243–249.
[32] N.N. Ruslan, N.A. Fadzlillah, A.H. Karim, A.A. Jalil, S. Triwahyono, Appl. Catal. A Gen. 406 (2011) 102–112.
[33] M. Santikunaporn, J.E. Herrera, S. Jongpatiwut, D.E. Resasco, J. Catal. 228 (2004) 100–113.
[34] S.N. Timmiati, A.A. Jalil, S. Triwahyono, H.D. Setiabudi, N.H.R. Annuar, Appl. Catal. A Gen. 459 (2013) 8–16.
[35] M.G. Falco, S.A. Canavese, R.A. Comelli, Appl. Catal. A Gen. 201 (2000) 37–43.
[36] R. Prins, Chem. Rev. 112 (2012) 2714–2738.
[37] D. Kubička, N. Kumar, T. Venäläinen, H. Karhu, I. Kubičková, H. Österholm, D.Y. Murzin, J. Phys. Chem. B 110 (2006) 4937–4946.
[38] H. Hattori, Stud. Surf. Sci. Catal. 138 (2001) 3–12.
[39] R. Monteiro, C.O. Ania, J. Rocha, A.P. Carvalho, A. Martins, Appl. Catal. A Gen. 476 (2014) 148–157.
[40] A. Katrib, A. Benadda, J.W. Sobczak, G. Maire, Appl. Catal. A Gen. 242 (2003) 31–40.
[41] H.D. Setiabudi, A.A. Jalil, S. Triwahyono, J. Catal. 294 (2012) 128–135.
[42] S. Triwahyono, A.A. Jalil, H. Hattori, J. Nat. Gas Chem. 16 (2007) 252–257.
[43] H. Al-Kandari, F. Al-Kharafi, A. Katrib, Catal. Commun. 9 (2008) 847–852.